RSC Advances

ROYAL SOCIETY OF CHEMISTRY

www.rsc.org/advances

Graphical Abstract

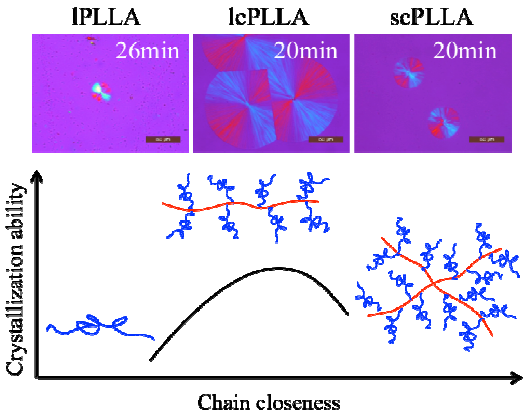

The crystallization ability of PLLA with different chain structure.

Facile Synthesis and Comparative Study of Poly(L-lactide) with Linear-Comb and Star-Comb Architecture

Xuefei Leng, Zhiyong Wei, Yingying Ren, Yang Li*, Yurong Wang, Qinyi Wang

In this work, two series of linear-comb and star-comb well defined graft poly(L-lactide) (PLLA) have been synthesized conveniently by one-pot ring-opening polymerization (ROP) of L-lactide using functionalized polybutadiene macroinitiators. The used organocatalyst of 1,8-diazabicyclo[5,4,0]undec-7-ene (DBU) allows the polymerization of L-lactide proceeds rapidly at room temperature. Kinetic studies of the ROP reaction in this system indicate a first-order kinetic in monomer concentration. ^{1}H NMR and GPC techniques are employed to characterize the synthesized polymers, validating the formation of desired comb structures with controllable chain length. Linear-comb and star-comb graft PLLA were comparatively studied as well as with linear PLLA by DSC and POM. The results reveal that comb structure makes a remarkable improvement of PLLA crystallization ability in both crystallinity and growth rate of spherulites. Furthermore, the more compacted star-comb structure imposes restriction on chain mobility, which weakens the growth effect to some extent. It is found that the glass transition temperature (T_g) and melting temperature (T_m) significantly depend on the side chain length and backbone structure. Rheological studies of both melt and instinct viscosity of the solution show that star-comb PLLA has the lowest hydrodynamic volume compared with linear-comb PLLA and linear PLLA.

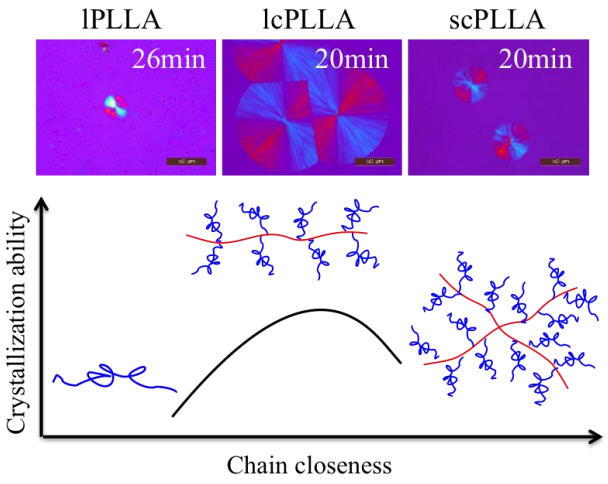

Address: State Key Laboratory of Fine Chemicals, Department of Polymer Science and Engineering, School of Chemical Engineering, Dalian University of Technology, Dalian 116024, Liaoning, China

Electronic Supplementary Information (ESI) available

Introduction

Polylactide (PLA) derived from renewable resources has drawn significant attention due to its well biodegradable/biocompatible properties and the other concerns associated with the use of petroleum-based products.[1-3] High molecular weight PLA and its copolymers are one of the most widely utilized polymers in the field of biomedical materials[4-8]. Due to the extremely high mechanical strength, it has been used as commodity and industrial materials as well as clinically in medical applications,[9-10] orthopaedic screw,[11-12] scaffolds,[13-15] etc. PLA can be directly prepared from lactic acid by polycondensation under azeotropic distillation conditions referred as poly(lactic acid)[16-18]. Ring-opening polymerization (ROP) of lactide is another effective route to synthesize PLA with higher molecular weight and lower polydispersity[19]. Stannous octoate ($Sn(Oct)_2$) is the most common catalyst for ROP of lactide[20]. However, tin based catalysts are less than ideal from both chemical and biological perspective. The organic catalysts now appear as viable substitutes for classical metallic catalysts[21-23]. Non-metallic ROP processes are demanded for sustainable and environmentally friendly products, especially in microelectronic[24] and biomedical[25-26] applications. In 2001, Hedrick et al. first reported N-heterocyclic carbenes as novel metal-free nucleophilic catalysts for the ROP of cyclic ester monomers[27]. Among those catalysts, the commercial available amidine and guanidine (such as 1,5,7-triazabicyclo[4,4,0]dec-5-ene (TBD) and 1,8-diazabicyclo[5,4,0]undec-7-ene (DBU)) provide better control of molecular weight and highly efficient at room temperature[28-29]. DBU has been used for ROP of cyclic carbonate and lactone monomers in the melt or in solution. Studies by mass spectrometry showed incorporation of DBU into the polycarbonate, suggesting a dual role as a pseudo-anionic catalyst and as an initiator[21,30-31]. However, the effect of multifunctional macroinitiator on the polymerization kinetic of lactide with DBU as catalyst has not received much attention.

The significance of the relationships between macromolecule architectures and their properties has recently been recognized. Different polymer structures such as star-shaped with several arm numbers[32-35], barbell-shaped[36-37], comb-shaped[38-39], and dendrimers[40-41] were synthesized. A lot of reports on the effect of branching, including branch structure and branch degree, showed that branching may accelerate or decelerate the crystallization process and influence the melting behavior[42-44] and the rheological properties[45-47]. Relatively, comb-shaped polymers were reported mainly on the synthesis rather than physical properties[48-50]. Ydens and coworkers used “grafting-from” technique to synthesize graft copolymers of poly(acrylates) and PLA. This technique required a preliminary synthesis of a backbone containing multiple initiator sites, which were synthesized by ATRP of MMA and HEMA using ethyl 2-bromoisobutyrate (EIBBR) as an initiator. Subsequent ROP of lactide from the obtained backbone[50]. Zhao et al. invested the morphology and thermal properties of a similar comb structure PLA. By comparing one comb PLLA sample (M_n = 80 kg mol^{-1}, PDI = 1.68) with linear PLLA, the results were not comprehensive to conclude the relationship between structure and properties[51]. Especially, how the backbone structure of comb polymer influence the polymer performance is unclear. The macromolecule structure is intended to affect the bulk viscosity and crystallization behavior of PLLA, which are critical aspects in terms of process ability and product properties.

In this work, we report a simplified synthetic approach for facile synthesizing graft polylactide utilizing DBU as catalyst by one-pot. The macroinitiators (polybutadiene-OH, PB-OH) with linear or star structure and controlled number of hydroxyl pending groups are firstly prepared according to our previous research work[52]. ROP of $_L$-lactide monomers from the as-obtained hydroxyl pending groups to give PLLA comb structures (Scheme 1).

Kinetic of the ROP reaction and the relationship between molecular weight and monomer conversion of this system were studied. Two series of well-defined linear-comb PLLA (lcPLLA) and star-comb PLLA (scPLLA) with different side chain length were synthesized. Both lcPLLA and scPLLA were designed in similar graft density in order to focus on the effects of the backbone architecture on crystallization ability, melting behavior and rheological property of PLLA. The objective of this work is to clarify the relations between the backbone structure and the physical properties of PLLA on the basis of observed phenomena.

Scheme 1. Synthesis of linear-comb and star-comb graft PLLA.

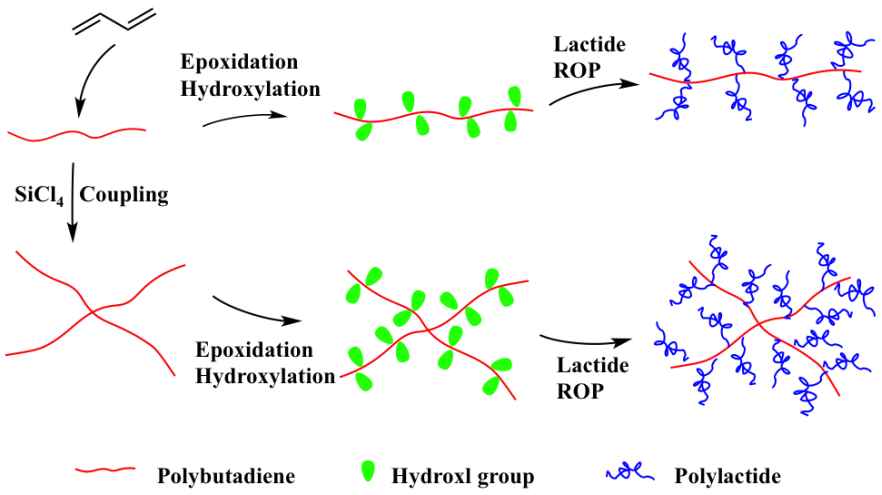

Experimental Section

Materials. Butadiene (Yanshan Petrochem. Co., polymerization grade) was treated with little of n-butyllithium (*n*-BuLi) to remove the moisture and inhibitor. *n*-BuLi (J&K Chemical, 2.5 M solution in n-hexane), was determined by Gilman-Haubein double titration and stored under 0 °C[53]. Tetrachlorosilane ($SiCl_4$, J&K Chemical, 98%), Dichloromethane (CH_2Cl_2, Aladdin), and Cyclohexane were distilled from CaH_2 under nitrogen. Tetrahydrofuran was dried over sodium benzophenone ketyl under nitrogen and freshly distilled. The terminating agent 2-propanol was degassed via three freezing-evacuation-thawing cycles. L-lactide (Alfa, 98%) were triple recrystallized from ethyl acetate respectively, then dried and stored in a glovebox. 1,8-Diazabicyclo[5.4.0]undec-7-ene (DBU, Sigma-Aldrich, 98%) was dried over calcium hydride, distilled under reduced pressure and stored in a glovebox. Trifluoromethanesulfonic acid (TfOH, Aladdin, 98%), Formic acid (HCOOH, Aladdin, 88%), Hydrogen peroxide (H_2O_2, 30%), and all other reagents were used as received from the commercial source without further purification.

Instrumentation. The molecular weight and PDI of the polymers were determined by GPC using a Waters 1515 HPLC pump, a Waters 2414 refractive index detector, and PS columns (one PL gel 5 μm10E4A and one Shodex KF805) in THF as eluent at a flow rate of 0.6 mL min^{-1} at 35 °C Calibration based on PS standards (Shodex PS STD SM-105). ^{1}H NMR spectra were record on a Bruker Avance 400 MHz spectrometer in $CDCl_3$ at 25-30 °C at a concentration of 4% w/v. The specific optical rotation, [*a*] of the polymer was measured in chloroform at a concentration of 1 g dL^{-1} at 25 °C using a JASCO J-810 Polari meter at a wavelength of 589 nm. Intrinsic Viscosity.

The intrinsic viscosities ([η]) of PLLA were determined in $CHCl_3$ by a 0.4mm Schott Ubbelohde viscometer at 30.0 °C. All samples were filtered before test. Flow time of the solvent and that of each of polymer solutions with four different concentrations below the overlap concentration c* were measured to determine [η] as described elsewhere[54]. The glass transition temperatures (T_g) and the melting temperatures (T_m) of the polymers were measured on differential scanning calorimeter (DSC, TA, Q520). Each sample was scanned in the range of 0 to 180 °C at a heating rate of 10 °C min^{-1} in aluminum pans under nitrogen atmosphere. Thermal history was removed by keeping the samples at 180 °C for 3 min. The crystalline morphology of the polymer was observed using a Leica DM4500P polarized optical microscopy (POM) equipped with a Linkam THMS420 hot stage. The PLLA samples were melted at 200 °C for 3 min to eliminate thermal history and then cooled to the isothermal crystallization temperature at a cooling rate of 40 °C min^{-1}. Then take the optical micrographs at appropriate times during the crystallization to examine the growth rate of PLLA spherulites. Rheological measurements were performed on a stress-controlled Rheometer AR2000 (TA Instruments Ltd.) equipped with parallel-plate geometry (diameter of 25 mm) and a gap of 1 mm at constant temperature 190 °C. Dynamic frequency sweep measurements were carried out in an oscillatory shear mode from 10 to 0.1 rad s^{-1}.

Synthesis of macroinitiator PB-OH

Synthesis of linear polybutadiene, followed by epoxidization and hydroxylation of epoxy groups (Scheme S1, and detailed polymerization condition is reported in supporting information). To synthesis the four arms star-shaped PB-OH, $SiCl_4$ was added as a coupling agent at the end of the polymerization of PB.

Ring opening polymerization of lactide

Synthesis of line-comb graft Poly($_L$-lactide) (lcPLLA). In a glovebox, a two-necked round bottom flask with macroinitiator (lPB-OH) (0.1 g, M_n = 4200 g·mol^{-1}, 0.024 mmol, 0.51 mmol OH) inside was previously dried by three azeotropic distillations with toluene[55]. Predetermined $_L$-lactide (11.36 g, 79 mmol, 2M) with CH_2Cl_2 were added first. Then injected DBU[56] (0.118 mL, 1 mol% relative to lactide) rapidly. The polymerization reaction proceeded at room temperature within 1h and was stopped by the addition of benzoic acid (0.183 g). The polymer was purified by precipitation with methanol twice and dried at 40 °C under vacuum to constant weight (yield > 98%). The reaction steps involved in the synthesis of lcPLLA copolymer are depicted in Scheme S2.

Synthesis of star-comb graft Poly($_L$-lactide) (scPLLA). To prepare scPLLA, use star-shaped sPB-OH as the macroinitiator instead of lPB-OH. The rest of the process was as same as that described for lcPLLA (yield > 98%).

Results and discussion

Linear and star-shaped PB-OH macroinitiators

To achieve the graft PLLA with the targeted molecular weight via "graft-from" strategy, the corresponding precursor linear and star-shaped backbone with controlled number of hydroxyl groups need to be prepared first. Since high molecular weight backbone precursor polymer was not necessary in this work, both linear and star-shaped PB were designed and synthesized with low molecular weight (M_n < 10 kg mol^{-1}).

Each procedure was characterized by GPC and ^{1}H NMR (Figure S1). In the epoxidation step, the ratio of $[1,4\text{-butadiene}]_0/[HCOOH]_0/[H_2O_2]_0$ was 1/0.4/0.5. Double bond with higher electron density favors the epoxidation, which is relatively less sensitive to steric effect[57]. It indicates that the epoxidation of PB occurred selectively at the 1,4-PB sites. The stirring efficiency is also important to control the epoxidation degree[58].

Accordingly, epoxidized PB (PBE) with no more than 20 mol% epoxidation degree was successfully obtained by controlling the addition of H_2O_2 with proper stirring rate. The degree of epoxidation were calculated by ^{1}H NMR (Figure S1(2)). In the hydroxylation step, epoxidized PB (PBE) in THF solution was treated with TfOH and H_2O to produce PB-OH ([epoxy group]$_0$/[TfOH]$_0$/[H_2O]$_0$/[THF]$_0$ = 1/0.83/15/30). Almost every epoxy group turned into two hydroxyl functionalities. The completion of reaction was confirmed by ^{1}H NMR spectrum (Figure S1(3)). GPC detected an expected small increase of molecular weight after the epoxidization and hydroxylation steps of PB. The characterization data for the initiators are summarized in Table 1.

Table 1. Characterization data of linear and star-shaped macroinitiators.

Macroinitiator	M_n[a] (g mol^{-1})	PDI[a]	Hydroxylation degree[b]	No.$_{OH}$ (mol^{-1})[c]
lPB-OH	4200	1.14	10.4%	13.4
sPB-OH	7800	1.28	11.2%	27.1

[a] Determined by GPC analysis with polystyrene standards. [b] Determined by the ^{1}H NMR (SI Figure 1). [c] [No.$_{OH}$] = e.g. (4200 / 58 × 90% × 10.4% × 2), where 58 g mol^{-1} was calculated as the average molecular weight of each PB-OH unit.

lcPLLA and scPLLA graft PLLA

Scheme S2 illustrates ROP of L-lactide with macroinitiator (lPB-OH) at following reaction conditions: [M]$_0$ = 1 mol L^{-1}, [M]$_0$/[OH]$_0$/[DBU]$_0$ = 70/1/0.7, at 25 °C. The conversion of monomer was determined with ^{1}H NMR, and the molecular weight and PDI of PLLA at different reaction time was measured by GPC (Figure S2 in SI). The reaction shows a standard first-order kinetic in monomer concentration (Figure 1(1)) and a linear relationship between molecular weight and monomer conversion (Figure 1(2)), which are characteristics of a living chain-growth polymerization[21]. This living chain-growth process also produces the polymerization with a high yield above 98% at room temperature within 1 hour. Another advantage of this organic base catalyst relies upon the fact that it acts as a bifunctional catalyst activation both monomers and hydroxyl group to give polymer narrow PDI. PDIs are fairly low (< 1.2) up to high monomer conversion, and even after prolonged reaction time. These results also demonstrated that undesirable transesterification reactions did not occur during the ROP reaction.

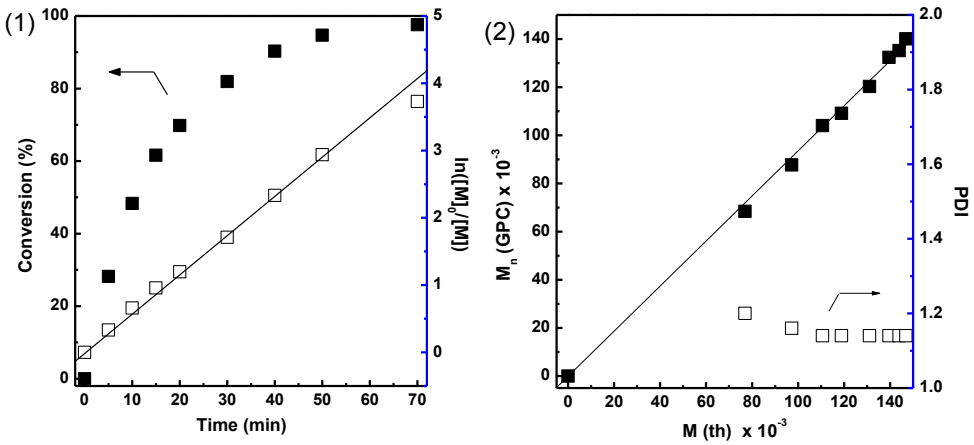

Figure 1. Conversion and ln([M]$_0$/[M]) versus time kinetic plot (1); and experimental M_n and PDI versus theoretical M_{th} (2); ROP of L-lactide in CH_2Cl_2 at 25 °C (Reaction conditions: [M]$_0$ = 1 mol L^{-1}, [M]$_0$/[OH]$_0$/[DBU]$_0$ = 70/1/0.7, macroinitiator: lPB-OH).

Two series of lcPLLA and scPLLA were synthesized by using lPB-OH and sPB-OH as the macroinitiators, respectively. Figure 2 shows GPC traces of macroinitiators and corresponding graft copolymers. The symmetric and narrow dispersed signals at longer retention time (RT) were PB-OH initiators, which were synthesized by anionic polymerization method. After ROP of lactide, the signals of initiators totally disappeared and the new signals appeared at shorter RT. It indicated that all of the initiators took part in ROP reaction and turned into graft copolymers. The peaks in Figure 2(1), which represent the lPB-OH and lcPLLA, are unimodal and quite narrow (PDI < 1.2). However, the four arms sPB-OH in Figure 2(2) turned out to be broader (PDI = 1.28) compared with lPB-OH after coupled by $SiCl_4$. The corresponding scPLLA also showed a broader PDI (< 1.4) than lcPLLA. Since the ROP reaction was finished efficiently and completely, no more separation was needed.

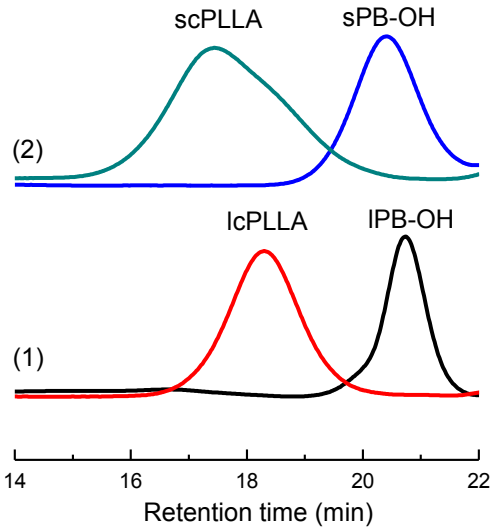

Figure 2. GPC traces of the macroinitiator and the graft PLLA after ROP: (1) lPB-OH and lcPLLA10; (2) sPB-OH and scPLLA10.

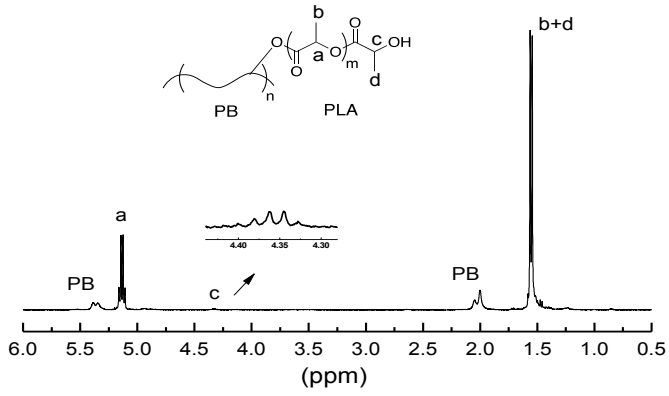

Figure 3. ^{1}H NMR spectra of graft PLLA (lcPLLA10).

The ^{1}H NMR spectrum of graft PLLA with assignments is shown in Figure 3. The major resonance signals a (at 5.14 ppm) and b (at 1.55 ppm) are attributed to PLLA. The methine proton signal (c, at 4.36 ppm) associated with the newly formed ester overlapped significantly with the PLLA end group. The resonance of PB main chain appeared when the graft PLLA molecular weight was low. To obtain comb copolymers with different molecular weights, the feed molar ratio of $_L$-LA and hydroxyl groups of PB-OH was varied. Assume that every hydroxyl group of PB-OH chains participate in initiation, the molecular weight of the resultant PLLA can be calculated from the integration ratio of the methine protons (a, at 5.14 ppm) next to the ester oxygen to the methine protons in the terminal hydroxyl groups.

The molecular weights and optical purities of the resultant lcPLLA and scPLLA were summarized in Table 2 and Table 3, respectively. The agreement of $M_{n,theo}$ and $M_{n,NMR}$ indicates that hydroxyl groups in PB-OH are effective initiating sites. In Table 2, the molecular weight of lcPLLA determined by GPC is close to its $M_{n,theo}$. In Table 3, $M_{n,GPC}$ of scPLLA is much lower than its $M_{n,theo}$. For same molecular weight, the hydrodynamic radii of graft polymer were smaller than that of linear one. The GPC values reflected the hydrodynamic radii of PLLA decrease when going from linear comb to the star comb architecture. This result did consistent with the trend of their intrinsic viscosity, which would be discussed following. By using DBU as a catalyst, an undesired racemization likely occurs because of the nucleophilic attacks on the activated monomers and the propagating species[59-60]. As a result, the decreases in optical purity would lower the crystallinity and mechanical properties of the obtained PLLA. Since the optical purities of all the PLLA, listed in Table 2 and Table 3, were similar about 90 % and still high. According to Tsuji et al., PLA can be crystalline when its OP is higher than 76%ee[61]. The comparative study between lcPLLA and scPLLA with different structure in this work are reasonable.

Table 2. Characterization data of lcPLLA macromolecules.

Sample	[OH][a]/[$_L$-LA]/[DBU]	$M_{n,theo}$[b] (kg mol^{-1})	$M_{n,NMR}$[c] (kg mol^{-1})	$M_{n,GPC}$[d] (kg mol^{-1})	PDI[d]	OP[e] (%)
lcPLLA10	1/10/0.1	23.9	24.4	25.0	1.19	91.1
lcPLLA30	1/30/0.3	62.8	61.2	58.4	1.15	91.3
lcPLLA50	1/50/0.5	119.9	118.3	116.6	1.18	89.6
lcPLLA70	1/70/0.5	140.6	139.6	137.1	1.14	89.8
lcPLLA100	1/100/0.5	198.9	191.5	198.6	1.16	90.1

[a] The mole of hydroxyl groups of lPB-OH. [b] $M_{n,theo}$ = [$_L$-LA]/[OH] × $M_{n,LA}$ × No.$_{OH}$ + $M_{n,PB\text{-}OH}$, where $M_{n,LA}$ is the molecular weight of LA and $M_{n,PB\text{-}OH}$ is the molecular weight of the lPB-OH (M_n = 4200 g mol^{-1}). [c] Determined by ^{1}H NMR (Figure 3). [d] Determined by GPC analysis with polystyrene standards. [e]Optical purity of PLLA.

Table 3. Characterization data of scPLLA macromolecules.

Sample	[OH][a]/[$_L$-LA]/[DBU]	$M_{n,theo}$[b] (kg mol^{-1})	$M_{n,NMR}$[c] (kg mol^{-1})	$M_{n,GPC}$[d] (kg mol^{-1})	PDI[d]	OP[e] (%)
scPLLA10	1/10/0.1	46.7	46.3	45.8	1.39	91.9

scPLLA20	1/20/0.2	85.6	84.1	78.1	1.38	90.8
scPLLA30	1/30/0.3	124.4	122.9	119.3	1.38	90.1
scPLLA40	1/40/0.4	163.3	148.2	132.2	1.39	91.1
scPLLA50	1/50/0.5	202.2	191.2	184.4	1.31	88.9

[a] The mole of hydroxyl groups of the sPB-OH. [b] $M_{n,theo}$ = [L-LA]/[OH] × $M_{n,LA}$ × No.$_{OH}$ + $M_{n,PB-OH}$, where $M_{n,LA}$ is the molecular weight of LA and $M_{n,PB-OH}$ is the molecular weight of the sPB-OH (M_n = 7800 g mol^{-1}). [c] Determined by ^{1}H NMR (Figure 3). [d] Determined by GPC analysis with polystyrene standards. [e]Optical purity of PLLA.

Properties of graft PLLA

It is well known that graft polyesters are different from their linear counterparts at physic-chemical properties owing to the molecular architecture. Well-designed star-shaped PB-OH backbone with exactly twice the number of hydroxyl groups of the linear PB-OH was synthesized in this research. The model could be described as: Numbers of PLLA chains grafted onto a central linear PB evenly, which resulted in lcPLLA; Two lcPLLA macromolecule crossed at middle of the comb backbone by chemical bonds, which resulted in scPLLA. These two new topological structures with linear or star-shaped backbone concentrated the PLLA chains by chemical bonds. For this model, the effect of different graft degree could be excluded in this work. The influence of the backbone structure was investigated by comparing the properties of the graft linear-comb/star-comb PLLA with a linear PLA, which was also an approach to prove their comb structure.

Intrinsic viscosity

The impact of the chain topology on the solution behavior was investigated by intrinsic viscosities measurement. It is well-know that intrinsic viscosity of a macromolecule is a reflection of its hydrodynamic volume in solution. For a given polymer and solvent system at a specified temperature, intrinsic viscosity ([η]) can be related to molecular weight through the following empirical equation known as the Mark-Houwink equation[62]:

$$[\eta] = K(Mv)^{\alpha} \quad (1)$$

where K and α are Mark-Houwink coefficients, and M_v is the viscosity-average molecular weight, which lies between M_n and M_w. If $[\eta]_{br}$ and M are measured for both the linear and the branched polymer, one can determine a branching factor (g') defined as:

$$g' = [\eta]_{br}/[\eta]_{l} \quad (2)$$

Table 4. Characterization data of PLLA macromolecules with different structures.

Sample	$M_{n,GPC}$ (kg mol^{-1})	PDI	η [a] (dL g^{-1})	η_{theo} [b] (dL g^{-1})	g' [c]
lPLLA10	1.9	1.16	0.08	0.09	
lPLLA50	7.1	1.25	0.23	0.23	
lPLLA400	46.8	1.42	0.91	0.90	
lPLLA800	114.7	1.51	1.71	1.74	
lcPLLA10	25.0	1.19	0.35	0.57	0.61

lcPLLA30	58.4	1.15	0.58	1.06	0.55
lcPLLA50	116.6	1.18	0.89	1.76	0.51
lcPLLA100	198.6	1.16	1.20	2.59	0.46
scPLLA10	45.8	1.39	0.46	0.89	0.51
scPLLA20	78.1	1.38	0.63	1.31	0.48
scPLLA30	119.3	1.38	0.78	1.79	0.44
scPLLA50	184.4	1.31	1.01	2.46	0.41

[a] Measured in $CHCl_3$ by a 0.4mm Schott Ubbelohde viscometer at 30°C. [b] Values of η_{theo} were calculated by the equation (1)[62], where K = 5.45, α = 0.73 the Mark-Houwink parameters. [c] Calculated by the equation (2).

To reveal the effect of the comb architecture, series of linear PLLA (M_n < 100 kg mol^{-1}) were synthesized with the same DBU catalyst by using benzyl alcohol as an initiator. Figure 4 shows Mark-Houwink plots for linear and graft PLLA measured in $CHCl_3$ by a 0.4mm Schott Ubbelohde viscometer at 30 °C and summarized in Table 4. Graft PLLA samples showed a significantly lower [η] than linear PLLA, although their M_n was much higher than that of the linear ones, confirming the comb architecture. In $CHCl_3$ solution, linear PLLA behave more rod-like, graft PLLA exhibit smaller hydrodynamic volumes[63]. For comb-shaped PLLA of the same molar mass (lcPLLA50 and scPLLA30), [η] and g' decrease slightly when going from linear comb to the star comb backbone architecture. This is consistent with a more compact structure in the highly branched star-shaped polymers[64-65]. The intrinsic viscosity decreases with the chain closeness increases.

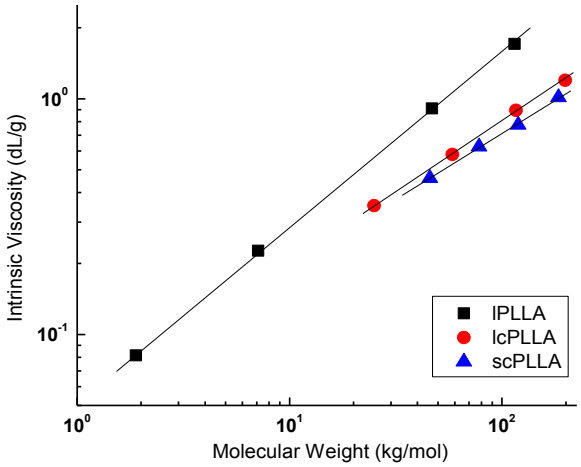

Figure 4. Intrinsic viscosities versus molecular weight of the linear PLLA (lPLLA), linear-comb PLLA (lcPLLA) and star-comb PLLA (scPLLA).

For the logarithmic plot (Figure 4), the straight line represents the equation:

$$\ln[\eta] = \ln K + \alpha \ln(M) \quad (3)$$

where K = 5.45, α = 0.73 are the Mark-Houwink parameters from reference. Mark-Houwink coefficients for comb graft PLLA can be calculated from the plot by equation (3), shown in Table 5. The synthesized linear PLLA samples with designed molecular weights showed similar K and α compared with literature values under the same test

condition. As a result, all linear and graft PLLA had similar value of *K*. The *α* values for graft PLLA were found to be lower. It decreases in the order lPLLA > lcPLLA > scPLLA, which parallels the order of increasing chain closeness.

Table 5. Mark-Houwink coefficients for PLLA/$CHCl_3$ system at 30 °C: lPLLA, lcPLLA and scPLLA.

	$lPLLA_{theo}$[a]	lPLLA	lcPLLA	scPLLA
$K \times 10^2$	5.45	5.12	5.19	5.36
α	0.73	0.74	0.60	0.56

[a] Mark-Houwink parameters from reference.

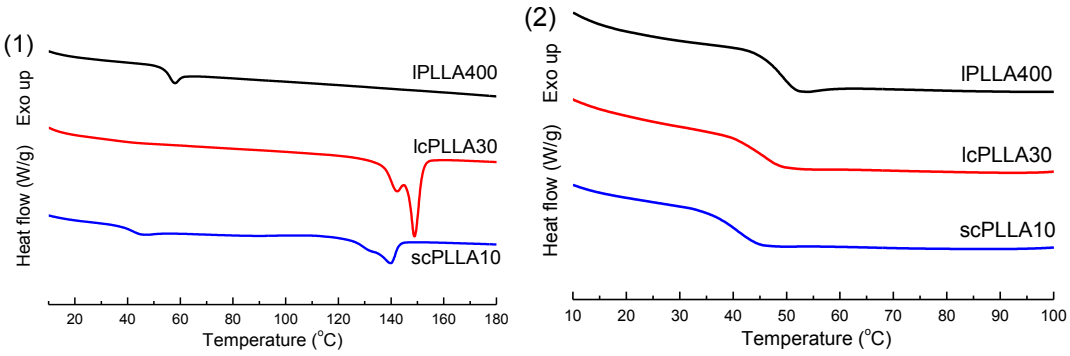

Figure 5. DSC curves of lPLLA, lcPLLA and scPLLA in second heating run: (1) The cooling rate is -2 °C min^{-1}; (2) The cooling rate is -10 °C min^{-1}.

Thermal properties

The DSC curves of linear, linear-comb and star-comb PLLA samples with similar molecular weights are shown in Figure 5 and the thermal transition data are collected in Table 5. Figure 5(1) presents the DSC thermograms at cooling rate of -2 °C min^{-1}. Linear PLLA did not show melting peak, agreed with its slow crystallization. The melting peaks of lcPLLA and scPLLA crystallites were presented with the crystallinity about 36.8% and 18.2% respectively, based on 93 J g^{-1} melting enthalpy of 100% crystalline PLLA[66]. This clearly shows a remarkable improvement in crystallization behavior of the graft PLLA compared with linear one. For the graft PLLA, the melting temperature (T_m) decreased from 149 °C of lcPLLA to 139 °C of scPLLA due to the increased segmental mobility of shorter side chains. The melting enthalpy (ΔH_m) also showed a decrease from 34.2 J g^{-1} to 17.0 J g^{-1}. Consequently, the crystallization ability is significantly improved by graft structure. However, more complicated topology structure star-comb PLLA with compact chains restricts the crystallization to some degree.

As seen in the Figure 5(1), lcPLLA showed no glass transition temperature (T_g) during the second heating cycle. Due to the slow cooling rate (-2 °C min^{-1}), lcPLLA chains formed compact crystallite, which restricted the segments movement. In addition, another heating cycle was conducted for same samples at a faster cooling rate (-10 °C min^{-1}) to observe T_g (Figure 5(2), T_{g2} in Table 6). The T_g of lcPLLA decreased slightly about 3.3 °C. At mean time, scPLLA showed a significant low T_g, which was 9.4 °C lower than that of lPLLA. There are two parameters that influence glass transition temperature when chain structure changed from linear to comb[67]. One is the free volume, which increases by the comb structure gives more flexible chain ends, contributes to decrease in T_g. The other is the segmental mobility, which decreases by chains are much closer and restricted in motion, contributes

to increase in T_g. Therefore, T_g may decrease or increase after grafted depending on which of the two counteracting parameters controls. Here, the T_g behavior of graft polymer is consistent with additional free volume from the increase in chain end. T_g and T_m of lcPLLA with different molecular weights are summarized in Table 7. For same backbone structure, T_g and T_m increase with M_n increases.

Table 6. Thermal properties of PLLA with different structure.

Sample	M_n (kg mol^{-1})	PDI	T_{g1}[a] (°C)	T_m[a] (°C)	ΔH_m[a] (J g^{-1})	X_c (%)	T_{g2}[b] (°C)
lPLLA400	46.8	1.42	53.9	-	-	-	50.1
lcPLLA30	58.4	1.15	-	148.8	34.2	36.8	46.8
scPLLA10	48.7	1.39	43.2	139.2	17.0	18.2	40.7

[a] T_{g1}, T_m, ΔH_m were measured by DSC, and estimated from Figure 5(1); [b] T_{g2} was estimated from Figure 5(2)

Table 7. Thermal properties of lcPLLA with different molecular weight.

Sample	M_n (kg mol^{-1})	PDI	T_g[a] (°C)	T_m[a] (°C)	G[b] (μm min^{-1})
lcPLLA10	25.0	1.19	42.0	147.9	1.39
lcPLLA30	58.4	1.15	44.8	148.8	0.48
lcPLLA50	116.6	1.18	50.7	151.2	0.32
lcPLLA70	137.1	1.14	51.2	151.0	0.17
lcPLLA100	198.6	1.16	54.6	154.8	0.11

[a] T_g, T_m were measured by DSC; [b] G, radium growth rate of spherulites: measured by POM at 110 °C, estimated by the plot in Figure S4.

Spherulite growth rate

To investigate the crystallization and morphology development of the graft lcPLLA, sample films were studied by optical microscopy under cross-polar conditions in isothermal mode. Representative crystal morphologies of lcPLLA10, lcPLLA50 and lcPLLA100 at 110 °C are shown in Figure 6. Compared with lcPLLA50 and lcPLLA100, lcPLLA10, with the lowest molecular weight, showed the biggest spherulites at the same crystallization time (40 min). Radium spherulite growth rate (G) could be calculated by the plot of radius versus crystallization time (Figure S4), summarized in Table 7. As a result, G decreases with M_n increases, due to the restriction of long chain mobility.

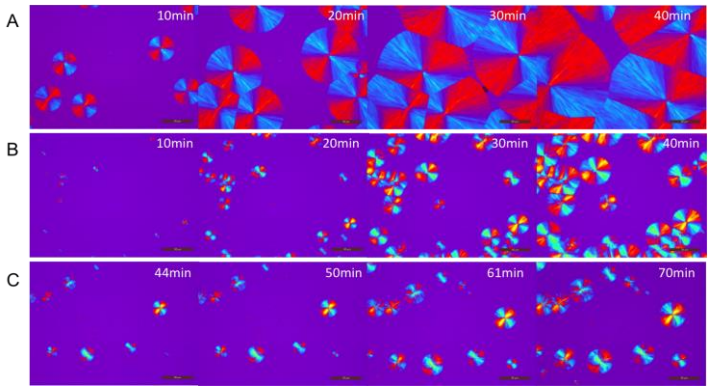

Figure 6. Selected POM micrographs during isothermal crystallization at T_c of 110 °C for lcPLLA samples of: (A) lcPLLA10, (B) lcPLLA50 and (C) lcPLLA100. The scale bar in the right bottom represents 50 μm and applies to all the micrographs. The crystallization time is indicated in the micrographs.

Effect of main chain structure on PLLA crystallization behavior was further investigated at different crystallization temperature. Figure 7 exemplifies the spherulite texture observed under cross-polars for linear PLLA and linear-comb/star-comb graft PLLA with similar molar mass at 120 °C. The typical negative spherulites with Maltese-cross pattern were detected for all samples, where ordered spherulites were seen. This strongly suggests that the comb chain structure in graft PLLA does not cause the macroscopic structural defects in the spherulites[42]. The sample lcPLLA10 showed both the largest size and the highest number of spherulites compared with other two samples at 120 °C after 20 min. The results indicate that comb structure highly improved crystallization property of PLLA at both nucleation and crystal growth. Nouri et al. also found that the present of branching points directly influenced the spherulite density by increasing the nucleation sites[67].

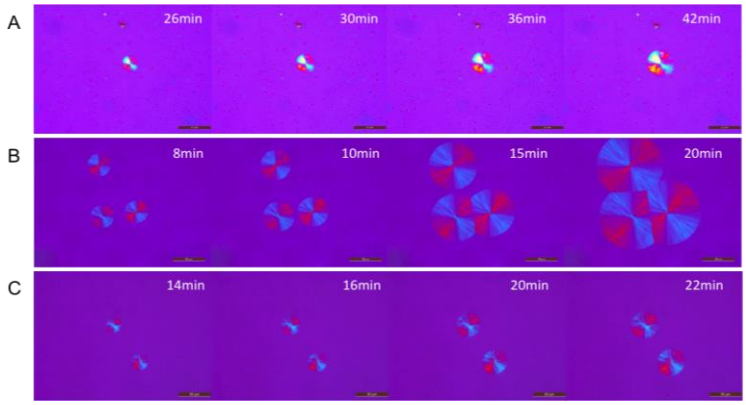

Figure 7. Selected POM micrographs during isothermal crystallization at T_c of 120 °C for the samples of: (A) lPLLA400, (B) lcPLLA30 and (C) scPLLA10. The scale bar in the right bottom represents 50 μm and applies to all the micrographs. The crystallization time is indicated in the micrographs.

The relation between Radius growth rate of spherulites (G) and crystallization temperature (T_c) is shown in Figure 8. G is significantly enhanced after changing the linear structure to comb structure at all T_c (from 100 °C to 130 °C). It is known that polymer crystallization take place under the confinement of side chains and main chains, and the

different confinement structure must greatly influences the crystallization behavior. For similar molar mass PLLA, molecular weight of each arm ($M_{n,arm}$) decreases with the number of arms increases. The lower $M_{n,arm}$ and the decreased bulk viscosity give graft PLLA side chains more mobility than linear PLLA. This confirmes the DSC result about the crystallization ability is significantly improved by comb structure. All these results indicate that the comb architectures do not alter the structures of PLLA crystallites, but markedly improve the crystallization behavior.

Along with the structure changed, the location of the highest growth rate also changed. The crystallization temperature, where G shows a maximum, ($T_{c\text{-}max}$), is given by an empirical formula[68]:

$$T_{c\,max} = 0.85T_m \quad (3)$$

Refer to the DSC results in Table 5, T_m of lcPLLA was 148.8 °C while for scPLLA was 139.2 °C. $T_{c\text{-}max}$ of lcPLLA was expected to be 126.5 °C and $T_{c\text{-}max}$ of scPLLA was expected to be 118.3 °C. The experimental results corresponded with the theoretical ones ($T_{c\text{-}max}$: lPLLA (about 130 °C) > lcPLLA (125 °C) > scPLLA (110 °C)). As a result, $T_{c\text{-}max}$ of graft PLLA, especially scPLLA, shifts to lower temperature owning to the decrease in T_m. The decreased $T_{c\text{-}max}$ of scPLLA will be a great benefit in industries, because actual processing is often carried out using water as a cooling medium.

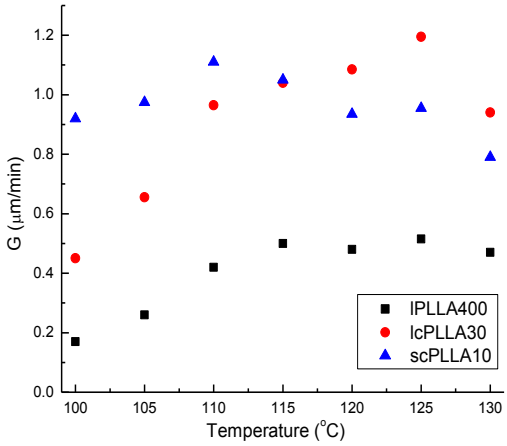

Figure 8. Radius growth rate of spherulites (G) versus crystallization temperature (T_c) for lPLLA400, lcPLLA30 and scPLLA10.

Rheological properties

Rheological properties of polymers are very sensitive to their topological structure[69]. In order to investigate the effect of the molecular structure on the chain mobility of PLLA, the melt rheological behavior was studied by a rheometer. Figure 9(1) shows the variation of complex viscosity as a function of the frequency at 190 °C for linear PLLA, lcPLLA and scPLLA. The scale of the frequency, from 0.01 Hz to 10Hz, is relatively low but the most sensitive region to reveal the difference of PLA chain structure[70]. It can be seen that lPLLA exhibits typical Newtonian behavior in the frequency region (lower than 10 Hz) and small shear thinning, which are characteristics for linear polymer.

To investigate the effect of chain structure, lPLLA800, lcPLLA50 and scPLLA30 with similar molecular mass (about 115 kg mol^{-1}, see Table 4) were picked. Both graft PLLA showed lower zero-shear viscosity than linear PLLA. The possible reason maybe the side chains are shorter compared with lPLLA and the closeness of the side chains reduce the volume of the graft PLLA. The shear thinning behavior is enhanced with tightening the side chains by changing chain structure from linear to comb[70]. The typical Newtonian plateau for linear PLLA disappeared and obvious shear thinning was observed for all graft PLLA. These results reveal that the compact chain structure significantly reinforces the melt. Similar results have been reported that branched PP has a more distinct shear thinning behavior than its linear polymer[71]. This trend is more obvious in lower side chain molecular weight (The degree of shear thinning: scPLLA10 > scPLLA30 > scPLLA50). Longer side chains weaken the effect of the backbone shape, since large side chains more seems to grow from a point than from a linear-shaped backbone or a star-shaped backbone.

For different structure graft PLLA with same molecular weight (M_n), compared lcPLLA30/scPLLA10 and lcPLLA100/scPLLA50, respectively. The star-comb graft polymer samples represented remarkable lower complex viscosity and decreased faster with the frequency increased. For graft PLLA with same molecular weight per one arm ($M_{n,arm}$), compared lcPLLA30/scPLLA30 and lcPLLA50/scPLLA50, respectively. Both of them showed similar complex viscosity although the total molecular weight of scPLLA was about twice that of the lcPLLA. This result indicates that $|\eta^*|$ is more depend on $M_{n,arm}$ than M_n. The four arms star backbone structure also enhanced the slop of the shear thinning obviously.

As a result, more closeness of the side chains, PLLA macromolecule shows much lower complex viscosity and becomes more sensitive to frequency. Besides the complex viscosity, the change of complex modulus, G^* with frequency is also sensitive to chain structure. In Figure 9(2), the values of G^* of linear PLLA and graft PLLA were decreased with increasing frequency, indicating a non-Newtonian behavior and pseudoplastic characteristics over the entire testing frequency range. G^* decreased with increased the closeness of side chains. The decrease trend of G^* was considered as similar as the complex viscosity showed in Figure 7(1). However, the slopes of the modulus curves of the graft PLLA decreased with the side chains got close. This more obvious nonterminal behavior for the graft PLLA than that of linear PLLA suggests a lower relaxation behavior, which can be ascribed to the formed graft points that restrain the long-range motions of polymer chains. The same decreases of the G^* and $|\eta^*|$ of the branched polymers (comb-shaped, long chain branched and H-shaped) also showed in some of the research at relatively low total molecular weights (M_w < 10 kg mol^{-1} for HDPE, M_w < 100 kg mol^{-1} for polybutadienes, M_w < 600 kg mol^{-1} for polystyrene)[72-74]. This result is different from the reported long chain branched PLLA[45-46,75]. Long chain branched PLLA exhibits increased G^* and $|\eta^*|$, which could be attributed to more side chain entanglement.

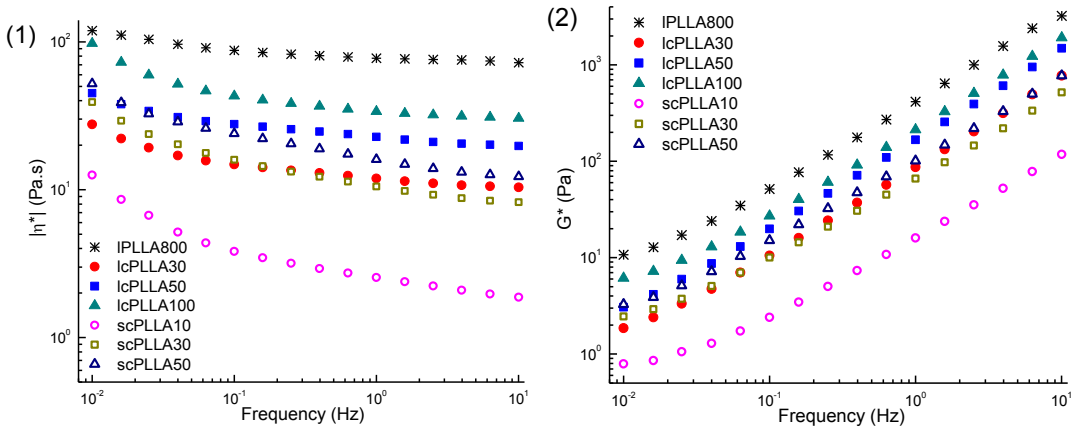

Figure 9. Variation of complex viscosity (1) and modulus (2) as a function of the frequency plots of linear and comb structure PLLA at 190 °C. lPLLA (lPLLA800-star), lcPLLA (lcPLLA30-cycles, lcPLLA50-squares, lcPLLA100-triangles), scPLLA (scPLLA10-opened cycles, scPLLA30-opened squares, scPLLA50-opened triangles).

Conclusions

Well-defined linear-comb and star-comb PLLA have been achieved by using functionalized macroinitiator and DBU as a catalyst in one-pot. Series of comb graft PLLA, with designed shape and number of side chains, could be controlled produced by changing the structure and the hydroxylation degree of PB-OH backbones. Both standard first-order kinetics in monomer concentration and the linear relationship between molecular weight and conversion approve that the ROP of lactide in this macroinitiator system is a living chain-growth polymerization. ^{1}H NMR and the GPC results shows molecular weights are proportional to the lactide/hydroxyl ratio. Linear-comb and star-comb graft PLLA were comparatively studied with linear PLLA. Intrinsic viscosity measurement confirms that the scPLLA displays the smallest hydrodynamic volumes in solution, due to the restricted chain mobility by grafting. T_g and T_m values of the graft PLLA were lowered owing to their non-linear architecture. Both DSC analysis and POM results indicated that the comb architectures didn't alter the structures of PLLA crystallites, but markedly improved the crystallization behavior, e.g. higher growth rate of spherulites and lower melting temperature. lcPLLA has the highest crystallinities, which indicates the more compacted comb structure of scPLLA presents steric hindrance of the graft points. Rheological measurements demonstrates that more closeness of the side chains, much lower complex viscosity and modulus the PLLA shows, which indicates the star-comb PLLA has the lowest complex viscosity and modules compared with its linear-comb and linear analogues at equal M_n (< 200 kg mol^{-1}). The shear thinning behavior is also enhanced with tightening the side chains.

The graft degree could also have important implications to properties of comb polymer. Detailed investigations of crystallization growth rate and rheological property are currently under way to determine the effect of graft degree within the same backbone structure.

Acknowledgements

This work was financially supported by National Program on Key Basic Research Program of China (973 Program No. 2015CB654700 (2015CB674701) and National Science Foundation of China (No. , 21174021, 21034001, and 31000427).

References

(1) Eling, B.; Gogolewski, S.; Pennings, A. J. *Polymer* **1982**, *23*, 1587.

(2) Rasal, R. M.; Hirt, D. E. *Macromol. Mater. Eng.* **2010**, *295*, 204.

(3) Hartmann, M. H. In *Biopolymers from Renewable Resources*; Kaplan, D., Ed.; Springer Berlin Heidelberg, 1998.

(4) Gupta, B.; Revagade, N.; Hilborn, J. *Prog. Polym. Sci.* **2007**, *32*, 455.

(5) Moon, S. I.; Lee, C. W.; Taniguchi, I.; Miyamoto, M.; Kimura, Y. *Polymer* **2001**, *42*, 5059.

(6) Inkinen, S.; Hakkarainen, M.; Albertsson, A.-C.; Södergård, A. *Biomacromolecules* **2011**, *12*, 523.

(7) Ignjatovic, N.; Uskokovic, D. *Appl. Surf. Sci.* **2004**, *238*, 314.

(8) BIOMATERIAL, O. *Advanced Drug Delivery* **2013**, 75.

(9) Bendix, D. *Polym. Degrad. Stab.* **1998**, *59*, 129.

(10) Gupta, A. P.; Kumar, V. *Eur. Polym. J.* **2007**, *43*, 4053.

(11) Kallela, I.; Tulamo, R.-M.; Hietanen, J.; Pohjonen, T.; Suuronen, R.; Lindqvist, C. *Journal of Cranio-Maxillofacial Surgery* **1999**, *27*, 124.

(12) Makarov, C.; Berdicevsky, I.; Raz-Pasteur, A.; Gotman, I. *J. Mater. Sci.: Mater. Med.* **2013**, *24*, 679.

(13) Zhang, R.; Ma, P. X. *Macromol. Biosci.* **2004**, *4*, 100.

(14) Kim, M. S.; Ahn, H. H.; Shin, Y. N.; Cho, M. H.; Khang, G.; Lee, H. B. *Biomaterials* **2007**, *28*, 5137.

(15) Pelto, J.; Björninen, M.; Pälli, A.; Talvitie, E.; Hyttinen, J.; Mannerström, B.; Suuronen Seppanen, R.; Kellomäki, M.; Miettinen, S.; Haimi, S. *Tissue Engineering Part A* **2012**, *19*, 882.

(16) Fukuzaki, H.; Yoshida, M.; Asano, M.; Kumakura, M.; Mashimo, T.; Yuasa, H.; Imai, K.; Hidetoshi, Y. *Polymer* **1990**, *31*, 2006.

(17) Tuominen, J.; Seppälä, J. V. *Macromolecules* **2000**, *33*, 3530.

(18) Fukuzaki, H.; Aiba, Y.; Yoshida, M.; Asano, M.; Kumakura, M. *Die Makromolekulare Chemie* **2003**, *190*, 1553.

(19) Carothers, W. H.; Dorough, G. L.; Natta, F. J. v. *J. Am. Chem. Soc.* **1932**, *54*, 761.

(20) Pitet, L. M.; Hait, S. B.; Lanyk, T. J.; Knauss, D. M. *Macromolecules* **2007**, *40*, 2327.

(21) Kamber, N. E.; Jeong, W.; Waymouth, R. M.; Pratt, R. C.; Lohmeijer, B. G. G.; Hedrick, J. L. *Chem. Rev. (Washington, DC, U. S.)* **2007**, *107*, 5813.

(22) Coulembier, O.; Moins, S.; Raquez, J. M.; Meyer, F.; Mespouille, L.; Duquesne, E.; Dubois, P. *Polymer Degradation and Stability* **2011**.

(23) Fèvre, M.; Vignolle, J.; Gnanou, Y.; Taton, D. In *Polymer Science: A Comprehensive Reference*; Editors-in-Chief: Krzysztof, M., Martin, M., Eds.; Elsevier: Amsterdam, 2012.

(24) Hedrick, J. L.; Magbitang, T.; Connor, E. F.; Glauser, T.; Volksen, W.; Hawker, C. J.; Lee, V. Y.; Miller, R. D. *Chemistry-A European Journal* **2002**, *8*, 3308.

(25) Seyednejad, H.; Ghassemi, A. H.; van Nostrum, C. F.; Vermonden, T.; Hennink, W. E. *J. Controlled Release* **2011**, *152*, 168.

(26) Kakuchi, T.; Chen, Y.; Kitakado, J.; Mori, K.; Fuchise, K.; Satoh, T. *Macromolecules* **2011**.

(27) Nederberg, F.; Connor, E. F.; Möller, M.; Glauser, T.; Hedrick, J. L. *Angewandte Chemie International Edition* **2001**, *40*, 2712.

(28) Lohmeijer, B. G. G.; Pratt, R. C.; Leibfarth, F.; Logan, J. W.; Long, D. A.; Dove, A. P.; Nederberg, F.; Choi, J.; Wade, C.; Waymouth, R. M.; Hedrick, J. L. *Macromolecules* **2006**, *39*, 8574.

(29) Pratt, R. C.; Lohmeijer, B. G. G.; Long, D. A.; Lundberg, P. N. P.; Dove, A. P.; Li, H.; Wade, C. G.; Waymouth, R. M.; Hedrick, J. L. *Macromolecules* **2006**, *39*, 7863.

(30) Joji, K.; Sylvain, K.; Dra?en, P.; Jean-Pierre, D.; Brigitte, B.; Frédéric, P.; Alain, D. In *Renewable and Sustainable Polymers*; American Chemical Society, 2011; Vol. 1063.
(31) Zhang, L.; Pratt, R. C.; Nederberg, F.; Horn, H. W.; Rice, J. E.; Waymouth, R. M.; Wade, C. G.; Hedrick, J. L. *Macromolecules* **2010**, *43*, 1660.
(32) Moravek, S. J.; Messman, J. M.; Storey, R. F. *Journal of Polymer Science Part A: Polymer Chemistry* **2009**, *47*, 797.
(33) Zhao, W.; Cui, D.; Liu, X.; Chen, X. *Macromolecules* **2010**, *43*, 6678.
(34) Ren, J.; Zhang, Z.; Feng, Y.; Li, J.; Yuan, W. *J. Appl. Polym. Sci.* **2010**, *118*, 2650.
(35) Perry, M. R.; Shaver, M. P. *Can. J. Chem.* **2011**, *89*, 499.
(36) Lu, D. D.; Yang, L. Q.; Shi, X. L.; Chang, Y.; Zhang, H.; Lei, Z. Q. *International Journal of Polymeric Materials and Polymeric Biomaterials* **2012**, *61*, 384.
(37) Zhao, R.-X.; Li, L.; Wang, B.; Yang, W.-W.; Chen, Y.; He, X.-H.; Cheng, F.; Jiang, S.-C. *Polymer* **2012**, *53*, 719.
(38) Yuan, F.; Pan, H.; Cheng, F.; Chen, Y.; Jiang, S.-C. *Polymer* **2012**, *53*, 2175.
(39) Wang, Q.; Wang, Y. *J. Polym. Res.* **2011**, *18*, 385.
(40) Ouchi, T.; Ichimura, S.; Ohya, Y. *Polymer* **2006**, *47*, 429.
(41) Atkinson, J. L.; Vyazovkin, S. *Macromol. Chem. Phys.* **2012**, *213*, 924.
(42) Sakamoto, Y.; Tsuji, H. *Polymer* **2013**, *54*, 2422.
(43) Sakamoto, Y.; Tsuji, H. *Macromol. Chem. Phys.* **2013**, *214*, 776.
(44) Phuphuak, Y.; Chirachanchai, S. *Polymer* **2013**, *54*, 572.
(45) Wang, L.; Jing, X.; Cheng, H.; Hu, X.; Yang, L.; Huang, Y. *Ind. Eng. Chem. Res.* **2012**, *51*, 10731.
(46) You, J.; Lou, L.; Yu, W.; Zhou, C. *J. Appl. Polym. Sci.* **2013**, *129*, 1959.
(47) Dean, K.; Petinakis, E.; Meure, S.; Yu, L.; Chryss, A. *J. Polym. Environ.* **2012**, *20*, 741.
(48) Ishizu, K.; Yamada, H. *Macromolecules* **2007**, *40*, 3056.
(49) Koutalas, G.; Iatrou, H.; Lohse, D. J.; Hadjichristidis, N. *Macromolecules* **2005**, *38*, 4996.
(50) Ydens, I.; Degée, P.; Dubois, P.; Libiszowski, J.; Duda, A.; Penczek, S. *Macromol. Chem. Phys.* **2003**, *204*, 171.
(51) Zhao, C.; Wu, D.; Huang, N.; Zhao, H. *Journal of Polymer Science Part B: Polymer Physics* **2008**, *46*, 589.
(52) Zhang, H.; Li, Y.; Zhang, C.; Li, Z.; Li, X.; Wang, Y. *Macromolecules* **2009**, *42*, 5073.
(53) Gilman, H.; Haubein, A. H. *J. Am. Chem. Soc.* **1944**, *66*, 1515.
(54) Gupta, A.; Kumar, V. *European polymer journal* **2007**, *43*, 4053.
(55) Gauthier, M.; Moeller, M. *Macromolecules* **1991**, *24*, 4548.
(56) Suriano, F.; Coulembier, O.; Dubois, P. *Reactive and Functional Polymers* **2010**, *70*, 747.
(57) Deubel, D. V. *The Journal of Organic Chemistry* **2001**, *66*, 3790.
(58) Yuan, Z.; Gauthier, M. *Macromolecules* **2005**, *38*, 4124.
(59) Shuklov, I. A.; Jiao, H.; Schulze, J.; Tietz, W.; Kühlein, K.; Börner, A. *Tetrahedron Lett.* **2011**, *52*, 1027.
(60) Coulembier, O.; Moins, S.; Raquez, J.-M.; Meyer, F.; Mespouille, L.; Duquesne, E.; Dubois, P. *Polym. Degrad. Stab.* **2011**, *96*, 739.
(61) Tsuji, H.; Ikada, Y. *Macromol. Chem. Phys.* **1996**, *197*, 3483.
(62) Mark, J. E. *Polymer Data Handbook*; Oxford University Press, 1999.
(63) Breitenbach, A.; Kissel, T. *Polymer* **1998**, *39*, 3261.
(64) Schappacher, M.; Deffieux, A. *Macromolecules* **2000**, *33*, 7371.
(65) Gauthier, M.; Tichagwa, L.; Downey, J. S.; Gao, S. *Macromolecules* **1996**, *29*, 519.

(66) Fischer, E. W.; Sterzel, H.; Wegner, G. *Kolloid-Z.u.Z.Polymere* **1973**, *251*, 980.
(67) Nouri, S.; Dubois, C.; Lafleur, P. G. *Journal of Polymer Science Part B: Polymer Physics* **2015**, *53*, 522.
(68) *Faraday Discussions of the Chemical Society* **1979**, *68*, 1.
(69) Janzen, J.; Colby, R. H. *J. Mol. Struct.* **1999**, *485–486*, 569.
(70) Zhou, M.; Zhou, P.; Xiong, P.; Qian, X.; Zheng, H. *Macromol. Res.* **2015**, *23*, 231.
(71) Su, F.-H.; Huang, H.-X. *J. Appl. Polym. Sci.* **2010**, *116*, 2557.
(72) Inkson, N. J.; Graham, R. S.; McLeish, T. C. B.; Groves, D. J.; Fernyhough, C. M. *Macromolecules* **2006**, *39*, 4217.
(73) Kraus, G.; Gruver, J. T. *Journal of Polymer Science Part A: General Papers* **1965**, *3*, 105.
(74) Roovers, J. *Macromolecules* **1984**, *17*, 1196.
(75) Liu, J.; Zhang, S.; Zhang, L.; Bai, Y. *Polymer* **2014**, *55*, 2472.